



HAL
open science

Europium spectroscopic properties impacted by femtosecond laser 3D nanostructuring in lithium niobium borosilicate glasses

Julien Ari, Maxime Cavillon, Olivier Plantevin, Matthieu Lancry, Bertrand Pournellec

► To cite this version:

Julien Ari, Maxime Cavillon, Olivier Plantevin, Matthieu Lancry, Bertrand Pournellec. Europium spectroscopic properties impacted by femtosecond laser 3D nanostructuring in lithium niobium borosilicate glasses. *Optical Materials: X*, 2022, 16, pp.100198. 10.1016/j.omx.2022.100198 . hal-04287703

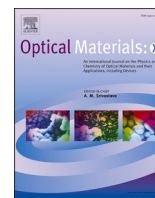
HAL Id: hal-04287703

<https://hal.science/hal-04287703>

Submitted on 15 Nov 2023

HAL is a multi-disciplinary open access archive for the deposit and dissemination of scientific research documents, whether they are published or not. The documents may come from teaching and research institutions in France or abroad, or from public or private research centers.

L'archive ouverte pluridisciplinaire **HAL**, est destinée au dépôt et à la diffusion de documents scientifiques de niveau recherche, publiés ou non, émanant des établissements d'enseignement et de recherche français ou étrangers, des laboratoires publics ou privés.



Europium spectroscopic properties impacted by femtosecond laser 3D nanostructuring in lithium niobium borosilicate glasses

Julien Ari^{a,*}, Maxime Cavillon^{a,**}, Olivier Plantevin^b, Matthieu Lancry^a, Bertrand Pommellec^a

^a Institut de Chimie Moléculaire et des Matériaux d'Orsay (ICMMO), Université Paris-Saclay, CNRS, 91405 Orsay, France

^b Laboratoire de Physique des Solides (LPS), Université Paris-Saclay, CNRS, 91405, Orsay, France

ARTICLE INFO

Keywords:

Femtosecond laser irradiation
Laser induced crystallization
Rare earth doped nanostructures
Rare earth doped glass
Borosilicate glass
Europium
Luminescence properties

ABSTRACT

We report in this article a study of luminescence properties of rare earth (herein Eu^{3+}) embedded in oriented nanostructures photo-induced by femtosecond laser irradiation in a lithium niobium borosilicate glass. A systematic comparison is made between the Eu^{3+} luminescence properties in the irradiated area and the glass matrix, including the effect of Eu^{3+} concentration on luminescence spectra, lifetimes and absorption/emission cross sections. Luminescence intensity is enhanced in the irradiated area compared to the glass matrix, which can be proved useful in optical devices engineering.

1. Introduction

Luminescent nanomaterials have emerged as an important field of research because they enable a large variety of applications including the design/development of miniaturized optical devices such as lasers and diodes [1–4]. Alongside, femtosecond (fs) laser direct writing (FLDW) technique to transform matter at the nanoscale is expanding to a large variety of materials, including photoluminescent materials in order to investigate new fluorescence properties in the irradiated glass to produce luminescent nanostructures [5]. As an example, visible emissions of doped glasses regain attractiveness from researchers for developing various optical materials who can be used as emission sources or 3D optical memories [6–9]. From this view, the crystallization in volume by FLDW is a promising method to induce oriented nanocrystals and nanostructures in glass materials, but the effect of the rare earth (RE) incorporation and associated photoluminescence properties upon laser irradiation is not established [10,11]. Recently, the fast crystallization of oriented LiNbO_3 nanocrystals has been demonstrated in $\text{Li}_2\text{O}-\text{Nb}_2\text{O}_5-\text{SiO}_2-\text{B}_2\text{O}_3$ (LNSB) glass system [12,13], proposing this glass matrix as a good candidate for photocrystallization [14,15]. The crystallographic orientation is considered identical compared to the non-doped LNSB but the role of RE dopant inside the oriented nanostructures depending on the fs laser parameters must be investigated [12,13]. The understanding of laser induced transformations on the

overall spectroscopic properties is a key requisite to the development of optically active devices at the nanoscale. Borate glasses are known to be a relatively good glass host for RE ions depending on the composition and the doping concentration, where the photoluminescence properties depends on the local environment [16,17]. Among the RE to investigate, Europium (Eu^{3+}) ions are commonly used to study local structure changes because of its relative simplicity of the energy diagram and a well-defined electric dipole transition $^5\text{D}_0 \rightarrow ^7\text{F}_2$ (around 615 nm) which allows to use it as an *in situ* spectroscopic probe to study the effect of the chemical environment around the ions [18,19]. Moreover, Eu^{3+} main photoluminescence emissions are located in the visible wavelength, which is convenient for luminescence characterization. Additionally, it is known that Eu^{3+} can be reduced to Eu^{2+} relatively easily upon fs laser irradiation due to the interaction of the RE^{3+} ions with the electron plasma induced at the focal point inside the glass matrix [20,21]. This makes difficult the control of photoluminescence properties of the RE ions in the irradiated region, as the homogeneity of the Eu^{3+} ions may be affected by the permanent photoreduction.

We report in this article the first study of Eu^{3+} luminescence properties measured in polarization-oriented crystallized nanostructures by fs laser irradiation of a glass material. The incorporation of Eu^{3+} ions into these oriented LiNbO_3 nanocrystals can produce a new kind of integrated and miniaturized optic materials (laser sources, sensors or high density optical storage) that will combine both non-linear optics with RE

* Corresponding author.

** Corresponding author.

E-mail addresses: julien.ari@universite-paris-saclay.fr (J. Ari), maxime.cavillon@universite-paris-saclay.fr (M. Cavillon).

spectroscopic properties in polarized sizable and orientable nanostructures. In this context, the objective of this article is to investigate the luminescence properties of a RE (e.g. Eu^{3+} ions) inside the irradiated area by fs-laser irradiation in LNSB doped glasses, and make a comparison of the luminescence properties with the doped glass matrix. First, Eu^{3+} absorption properties from the glass matrix will be presented, followed by photoluminescence and lifetime measurements from the Eu^{3+} in the irradiated area. The variations of absorption and emission cross sections are also presented.

2. Experimental details

The glass synthesis is realized from raw elements Li_2CO_3 (Alfa 5 N), Nb_2O_5 (Alfa, 3 N), SiO_2 (Alfa, 4 N), H_3BO_3 (Alfa, 4 N) and Eu_2O_3 (Alfa, 4 N). Three glasses of 20 g are prepared following the conventional melting-quenching method in atmospheric conditions. The host glass composition $33\text{Li}_2\text{O}-33\text{Nb}_2\text{O}_5-13\text{SiO}_2-21\text{B}_2\text{O}_3$ mol% is doped with 0.5 mol% Eu^{3+} (LNSB0.5Eu), 1 mol% Eu^{3+} (LNSB1Eu) and 2 mol% Eu^{3+} (LNSB2Eu). Dehydration and decarbonation steps are performed prior the melting at respectively 150 °C (30 min) and 1200 °C (30 min). Glasses are melted at 1400 °C in a platinum crucible during 1 h, then quenched between two stainless steel plates preheated at 350 °C. Glasses are annealed at 350 °C for 3 h, then slowly cooled down to room temperature using the thermal inertia of the oven. The obtained glasses are cut and polished down to optical quality and to 1 mm thickness slabs.

The irradiation of the glass is made following the same procedure as already describe elsewhere [12,15]. In short, a femtosecond laser beam, operating at 1030 nm, is focused inside the glass at 300 μm depth in air using an aspherical lens (NA = 0.6). A three-axis motorized translation stage is used to control the motion of the sample during the irradiation. 1 mm long lines are written inside the glasses at 800 fs, 200 kHz, and a fixed writing speed of 10 $\mu\text{m}/\text{s}$. A static irradiation step is performed before laser scanning to trigger crystallization [13]. Energies ranging from 0.1 to 1.2 μJ are investigated using two writing polarization configurations (labeled 0° and 90° as relative to the writing direction orientation). A minimum spacing of 20 μm between each line is used. After irradiation, the samples are polished in the cross section in order to bring the irradiated lines at the surface of the glass for luminescence measurements. As Eu^{3+} is photoluminescent in the visible range, it can be observed in the irradiated area using an adapted excitation source and an optical microscope in reflection mode.

The photoluminescence spectra are measured using an Olympus BX51 microscope and a spectrophotometer QuantaMaster Horiba Jobin-Yvon equipped with two fiber-connected laser sources, with centered wavelengths of 375 and 454 nm. The excitation spectrum is recorded for an emission at 615 nm. The excitation wavelength (λ_{ex}) of 375 nm is used and focused on the sample using a 50x microscope objective (MO50x), and the luminescence spectra are collected using a Hamamatsu PM13456 photomultiplier tube. The laser spot size is estimated to be around 10 μm in diameter at the focal point. All spectra measurements are performed in the cross section of the irradiated glasses. The decay curves of the Eu^{3+} ${}^5\text{D}_0 \rightarrow {}^7\text{F}_2$ (615 nm) and ${}^5\text{D}_1 \rightarrow {}^7\text{F}_1$ (542 nm) transitions are recorded using the SSTD (Single Shot Transient Digitizer) technique and a pulsed 454 nm fiber laser excitation at a frequency of 20 Hz for both glass matrix and irradiated area. The signal is collected with a monochromator Jobin Yvon HR250 and the photomultiplier tube. The emission cross sections $\sigma_{\text{em}}(\lambda)$ are then calculated from the fluorescence lifetime measurements and the FWHM (full width at half maximum) of the normalized luminescence transitions using the Füchtbauer-Ladenburg equation [22].

The optical absorption spectra are recorded using a Carry 5000 spectrometer in the Visible/Near Infrared wavelengths and a Fourier-transform infrared spectroscopy (FTIR) Vertex 70 Bruker setup for the infrared (IR) wavelengths. Absorbance spectra are measured on double side optical polished bulk samples of 1 mm thickness. The absorption coefficients $\alpha(\lambda)$, and absorption cross sections $\sigma_{\text{abs}}(\lambda)$ are calculated

from the recorded spectra.

Finally, high resolution Titan³ G2 80–300 (FEI Thermo Fisher Scientific) scanning transmission electron microscopy (STEM) at 200 kV is used for nanoscale imaging and to determine the repartition of the Eu atoms in the laser irradiated area. This experiment is made on a 100 nm thickness sample slice prepared using a focus ion beam (FIB) Helios 660 scanning electron microscope (SEM) and selected in the laser writing direction. Elemental analysis of Eu is performed using energy dispersive x-ray spectroscopy (EDS).

3. Results and discussions

The absorption coefficients for the three doped glasses are presented at Fig. 1 (a), with the excitation spectrum of LNSB0.5Eu glass matrix in inset image. The Eu^{3+} absorption and emission energy diagrams containing the observed transitions are respectively presented in Fig. 1(b) and (c), adapted from Ref. [17]. The main absorption transitions from the Eu^{3+} are located near the bandgap at 357 nm ($E_g = 3.48$ eV) of the LNSB host glass, making these transitions difficult to extract from the absorption measurements.

The strongest transitions observed in Fig. 1(a) are attributed to the absorption of Eu^{3+} ground state ${}^7\text{F}_0$ to the excited levels ${}^5\text{L}_6$ (394 nm) and ${}^5\text{D}_2$ (465 nm). Two other transitions are observed at 400 and 415 nm, which respectively correspond to ${}^7\text{F}_1 \rightarrow {}^5\text{L}_6$ and ${}^7\text{F}_1 \rightarrow {}^5\text{D}_3$ absorptions. Two additional weak transitions are observed at 526 and 533 nm corresponding respectively to ${}^7\text{F}_0 \rightarrow {}^5\text{D}_1$ and ${}^7\text{F}_1 \rightarrow {}^5\text{D}_1$ (Fig. 1(b)). The highest absorption coefficient is observed at 394 nm for the transition ${}^7\text{F}_0 \rightarrow {}^5\text{L}_6$ ($\alpha \approx 4.5$ cm^{-1}). Finally, two other absorption transitions are observed in the near IR region at 2.088 μm and 2.203 μm that correspond respectively to the ${}^7\text{F}_0 \rightarrow {}^7\text{F}_6$ and ${}^7\text{F}_1 \rightarrow {}^7\text{F}_6$ splitting of the fundamental multiplet level [19]. The transitions below 390 nm cannot be clearly attributed because the bandgap absorption is already dominating from these wavelengths. Nevertheless, some transitions can be resolved from the excitation spectrum (inset image Fig. 1(a)), as for example the ${}^7\text{F}_0 \rightarrow {}^5\text{G}_3$ transition at 380 nm. This transition is matching the wide excitation spectrum of Eu^{2+} corresponding to $4f^7 \rightarrow 4f^6 5d^1$ transition, thus making an excitation at around 380 nm (375 nm for the laser used) more suitable for simultaneous excitation compared to 394 nm, if Eu^{3+} reduction is happening upon fs laser irradiation. Indeed the excitation spectrum for the Eu^{2+} ions is reported in the literature and shows a large absorption band between 250 and 400 nm [23,24]. The photoluminescent emission transitions observed under 375 nm excitation are presented in Fig. 1(c). The six main emissions are observed at 542, 579, 591, 615, 650 and 700 nm and corresponds respectively to the transitions ${}^5\text{D}_1 \rightarrow {}^7\text{F}_1$, ${}^5\text{D}_0 \rightarrow {}^7\text{F}_0$, ${}^5\text{D}_0 \rightarrow {}^7\text{F}_1$, ${}^5\text{D}_0 \rightarrow {}^7\text{F}_2$, ${}^5\text{D}_0 \rightarrow {}^7\text{F}_3$ and ${}^5\text{D}_0 \rightarrow {}^7\text{F}_4$.

Fig. 2(a) shows the variation of luminescence intensity between the irradiated area at 1 μJ and the pristine (i.e., non-irradiated) glass matrix, that is $\Delta I(\lambda) = [I_{\text{irradiated area}}(\lambda) - I_{\text{glass matrix}}(\lambda)]$. Each spectrum is normalized with respect to its highest intensity peak at 615 nm preceding the calculation of $\Delta I(\lambda)$. The excitation wavelength is fixed at 375 nm, with a delivered laser power set to 5 mW. The laser beam is focused at the surface on the sample cross section containing the lines. It is worth pointing out that even though the luminescence is increased at 542 nm, the main transition at 615 nm is still the most intense from the full spectrum. The Eu^{3+} concentration is affecting the presence of photo-reduced Eu^{2+} on the luminescence spectrum. Indeed this phenomenon was already observed in the literature, where lower Eu^{3+} concentration involves more photoreduction in proportion from 0.5 mol% Eu^{3+} to 0.05 mol% Eu^{3+} in a sodium borate glass [21]. This explains why the signature of Eu^{2+} ions is more pronounced in LNSB0.5Eu compared to LNSB1Eu and LNSB2Eu, with the production of a finite number of electrons trapped in Eu^{3+} sites during fs laser irradiation for a given energy.

By comparing the variation of the emission spectra presented at Fig. 2(a), the main difference arises from the transition centered at 542 nm (${}^5\text{D}_1 \rightarrow {}^7\text{F}_1$). It worth mentioning here that the intensity of this transition decreases when Eu^{3+} concentration increases from 0.5 to 2

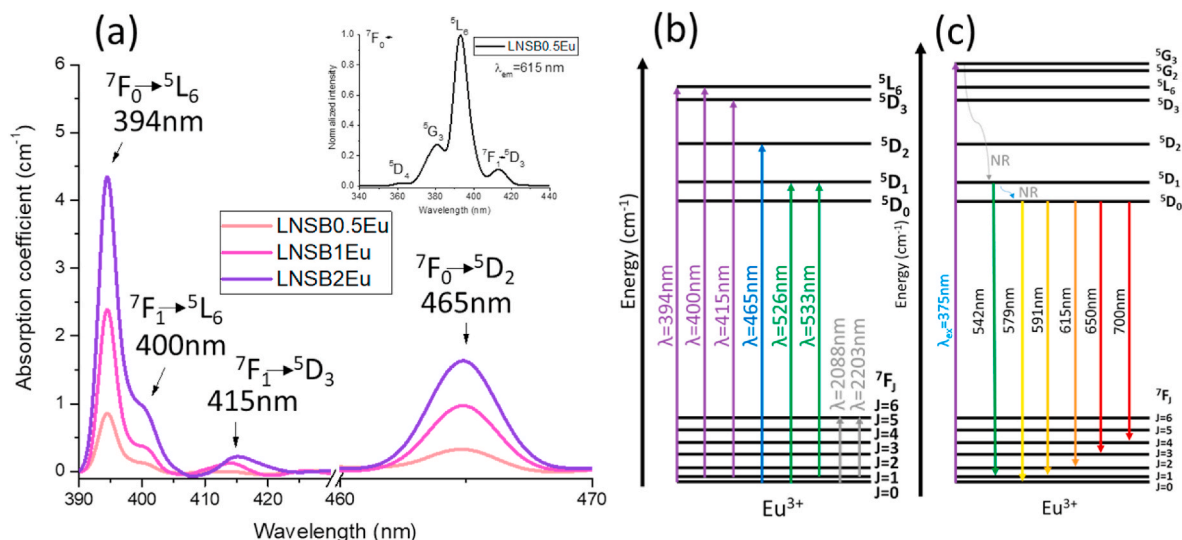


Fig. 1. (a) Absorption coefficients $\alpha(\lambda)$ of the LNSB doped glasses (0.5, 1 and 2 mol% Eu^{3+}). Inset image is the excitation spectrum of LNSB0.5Eu glass matrix (for an emission at 615 nm). (b) Eu^{3+} energy diagram with the observed absorption transitions. (c) Eu^{3+} energy diagram with the observed emission transitions. Diagrams are adapted from Ref. [17].

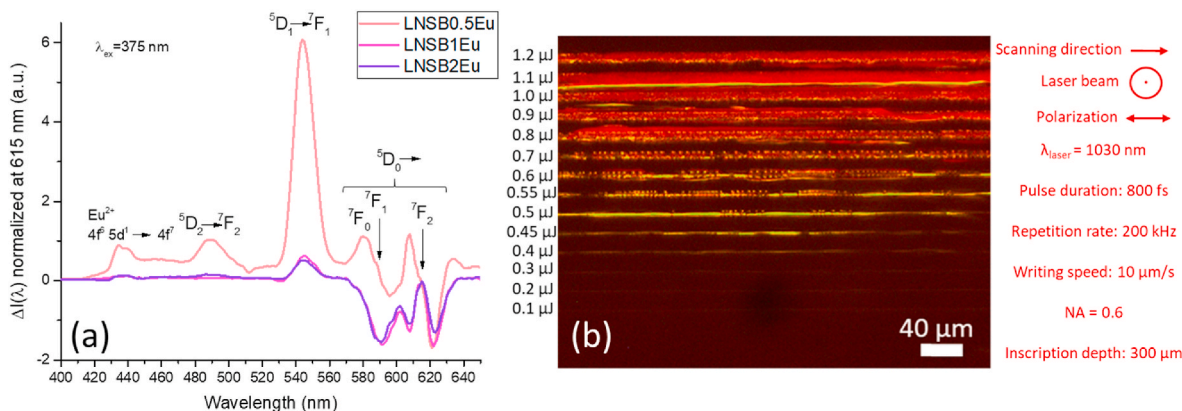


Fig. 2. (a) Variation of emission intensities $\Delta I(\lambda)$ between the irradiated areas made at 1 μJ and the glass matrices for the LNSB doped glasses (data are normalized at 615 nm) measured on the cross section. (b) Optical microscope image of the irradiated lines taken from the top surface of LNSB0.5Eu in reflection mode under non-polarized 366 nm UV lamp illumination. Fixed laser parameters: 1030 nm, 800 fs, NA = 0.6, 200 kHz, 0° polarization, 10 $\mu\text{m/s}$ and 300 μm inscription depth.

mol%. Overall, the spectra from the irradiated area and the glass matrix have the same radiative emission transitions although with varying intensities. The largest increase of luminescence intensity is observed on the ${}^5\text{D}_1 \rightarrow {}^7\text{F}_1$ (542 nm) transition in the irradiated region, as shown in Fig. 2(a). This trend is more pronounced in LNSB0.5Eu compared to LNSB1Eu and LNSB2Eu irradiated samples, likely due to Eu^{3+} concentration quenching. Overall, the luminescence is enhanced for LNSB0.5Eu excepted at 591 nm (${}^5\text{D}_0 \rightarrow {}^7\text{F}_1$) and 615 nm (${}^5\text{D}_0 \rightarrow {}^7\text{F}_2$) where the FWHM are reduced. Fig. 2(b) shows the microscope image in reflection mode of the LNSB0.5Eu irradiated sample illuminated with an UV lamp emitting at 366 nm. This picture of the irradiated lines shows a red (${}^5\text{D}_0 \rightarrow {}^7\text{F}_2$ at 615 nm) and yellow (${}^5\text{D}_0 \rightarrow {}^7\text{F}_0$ at 579 nm) luminescence throughout the sample coming from the Eu^{3+} ions. The variations of compositions induced by elemental migrations during the irradiation are affecting the luminescence intensities of Eu^{3+} . These ions are dispersed throughout the sample, both in the irradiated area and glass matrix. The contrast is due to light scattering inside the laser tracks. Under natural light in transmission mode, the irradiated areas would appear dark because of their relatively large thicknesses and the significant light scattering. Therefore, this observation methodology is more convenient to investigate the laser track morphologies in these specific experimental conditions.

The luminescence from the irradiated lines made at 0° and 90° polarization conditions did not show noticeable difference on the spectrum, and therefore no effect of the writing polarization seems to affect the photoluminescence properties of Eu^{3+} in the experimental conditions. The variation of pulse energy slightly modifies the emission spectra, as the only detected difference is a small increase of the intensity at 591 nm with the pulse energy. However, this variation cannot be fully attributed to the change in pulse energy because of the small size (typically between 2 and 10 μm) of the irradiated area for energies below 0.9 μJ , which suppose that a fraction of the glass matrix is excited simultaneously (~10 μm laser spot diameter). Therefore, the impact of pulse energies on luminescence properties cannot be reliably elucidated with this study.

A negligible quantity of Eu^{2+} is also detected in the pristine. This is attributed to the reduction of Eu^{3+} during the glass synthesis, as it is described in the literature in non-reducing atmosphere [25–27]. This concentration of Eu^{2+} can vary by controlling the environment during the melting of the glass but it is always observed in both inert or oxidizing atmosphere and is attributed to electron charge compensation transfers between the host lattice and the RE^{3+} ions.

Fig. 3 shows the results of the STEM analysis performed on an irradiated area at 1 μJ in LNSB1Eu. The presence of pseudo-lamellar nanostructures is clearly visible on Fig. 3(a). The migration of Eu^{3+}

ions is observed using STEM/EDS mapping and reported in Fig. 3(b). The presence of Eu^{3+} clusters confirms the luminescence quenching observed for LNSB1Eu and LNSB2Eu. The Eu^{3+} is found in both $\text{SiO}_2\text{-B}_2\text{O}_3$ glass phase and LiNbO_3 crystals. Interestingly, a migration of Eu^{3+} ions is observed from the irradiated area towards the interface with the pristine, characterized by an increase of Eu^{3+} concentration at the interface and a depletion of Eu^{3+} in the irradiated area near the interface. This elemental migration can be attributed to a higher temperature in the center of the irradiated region, where the Eu^{3+} ions are going toward the coolest region (positive Soret effect), thus creating a shell-like structure of Eu^{3+} ions [28]. For completeness, the Eu^{3+} concentration at the center of the irradiated spot only show small fluctuations, as sometimes the pristine glass phase remains in some local regions. The partial crystallization makes it difficult to observe these variations at the center of the irradiated area. In the experimental conditions provided, only the migration at the edge of the crystallized area has been observed, where we assume that Eu^{3+} ions have the time to migrate toward the coldest region during the irradiation.

Lifetime measurements performed on the emissions at 615 nm ($^5\text{D}_0 \rightarrow ^7\text{F}_2$) and 542 nm ($^5\text{D}_1 \rightarrow ^7\text{F}_1$) are presented in Table 1, along with absorption and emission cross sections. σ_{abs} is calculated using the relations presented in the caption of Table 1. We assume constant refractive indices of 1.94 for the glass matrices and 1.96 for the irradiated areas at 633 nm [29].

The maximum absorption cross-section is measured at 394 nm for LNSB2Eu, where $\sigma_{\text{abs}} = 1.56 \times 10^{-20} \text{ cm}^2$. The measured fluorescence lifetimes at 542 and 615 nm are both lower in the irradiated area compared to the glass matrix for the three glasses. The maximum lifetimes are observed for LNSB0.5Eu at 615 nm, with measured values of 769.4 μs for the glass matrix and 690.7 μs for the irradiated area (estimated experimental error $\pm 0.1 \mu\text{s}$). The calculated emission cross sections at 615 nm are higher in the irradiated areas, as the highest σ_{em} is recorded at $4.7 \times 10^{-21} \text{ cm}^2$ for LNSB2Eu. The emission cross section at 542 nm is also higher of about 9% on average in the irradiated area compared to the glass matrix (maximum at $19.2 \times 10^{-20} \text{ cm}^2$ for LNSB0.5Eu) and is decreasing when the Eu^{3+} concentration is increased from 0.5 to 2 mol%.

According to Ref. [21], photoreduction of Eu^{3+} induced by fs laser irradiation is observed on the photoluminescence spectrum when enough laser power and exposure time are used for Eu^{3+} concentrations between 0.05 and 0.5 mol%, but it is not inducing crystallization at the focal point in the sodium borate glass matrix. Photoreduction interaction comes from the electron plasma formed in the irradiated glass but the phenomenon does not appear dominant in LNSB:Eu $^{3+}$ because of the relatively high Eu^{3+} concentrations used (from 0.5 to 2 mol%). Partial energy transfers can take place from the broad Eu^{2+} luminescence because Eu^{3+} excitation wavelength at 394 nm and 415 nm are matching the Eu^{2+} emission, but the maximum intensity of the $4f^6$

$5d^1 \rightarrow 4f^7$ transition at around 430 nm is not affected by the reabsorption phenomenon. The quantity of Eu^{2+} ions induced by fs laser irradiation is low for 1 and 2 mol% Eu^{3+} concentrations. For these two glasses, the photoluminescence variations of Eu^{2+} ions have a similar shape at 430 nm for a given composition (Fig. 2(a)), confirming the proportion of photoreduced Eu^{3+} at the focal point is not significant compared to lower Eu^{3+} concentrations. Therefore it is challenging to ascribe unambiguously any structural changes around the ion, which can be influenced by the homogeneity of the photoreduction process [21]. The amount of Eu^{2+} formed during the synthesis appears negligible for the three investigated glasses. No effect of the writing polarization orientation is found neither on the luminescence spectrum or on the lifetime values. The decrease of the $^5\text{D}_1 \rightarrow ^7\text{F}_1$ luminescence with the increase of Eu^{3+} concentration is attributed to luminescence quenching. The increase of luminescence in the irradiated area can be likely attributed to a combination of Eu^{3+} from both $\text{SiO}_2\text{-B}_2\text{O}_3$: Eu^{3+} glass phase and LiNbO_3 : Eu^{3+} nanocrystals, as this statement is confirmed by the observations made from STEM/EDS analysis.

Lifetime measurements suggest that the Eu^{3+} ions are in different chemical environments with respect to laser induced crystallization and elemental migration. By comparing to the literature [30,31], the lifetimes measurements of Eu^{3+} performed on silica containing glasses show higher values than LNSB:Eu $^{3+}$ doped samples synthesized in this study. For instance, A. Herrmann et al. [30] have shown lifetimes of 2–3 ms for Eu^{3+} at 612 nm ($^5\text{D}_0 \rightarrow ^7\text{F}_2$). These values are measured in borosilicate based glasses containing high concentration of silica (more than 74 mol.% of SiO_2) and low alkali content (less than 16 mol.% Na_2O) compared to the LNSB which contains 13 mol.% of SiO_2 and 33 mol.% of Li_2O . Therefore, structural differences as an increase of non-bridging oxygen and a more ionic bonding character are expected surrounding the Eu^{3+} ions (SiO_4 , BO_4 and BO_3 groups), yielding to lower lifetime values. They also show that the lifetime is independent from the doping concentration in the commercial Duran glass (even when phase separation is observed) but this phenomenon is not observed in LNSB:Eu $^{3+}$ glasses, as the lifetimes are decreased when the Eu^{3+} concentration is increased up to 2 mol%. This proves that the time resolved fluorescence is strongly dependent of the glass composition, thus the local environment of the ions even in the same glass family (here, borosilicate based glasses). They also demonstrate that Eu^{3+} doped Duran glass shows two lifetimes contributions at 612 nm when fitting the decay curve, corresponding to two different environments but this aspect is not observed in LNSB:Eu $^{3+}$ glasses. A. Sreenivasulu et al. have measured a lifetime of 0.47 ms for LiNbO_3 : Eu^{3+} doped crystals [31], this value is lower than the irradiated areas in LNSB:Eu $^{3+}$ doped glasses and can be explained by the fact that they are partially crystallized with an inhomogeneous distribution of Eu^{3+} ions, as observed in Fig. 3(b).

As $^5\text{D}_0 \rightarrow ^7\text{F}_2$ is an electric dipole transition, it is very sensitive to the

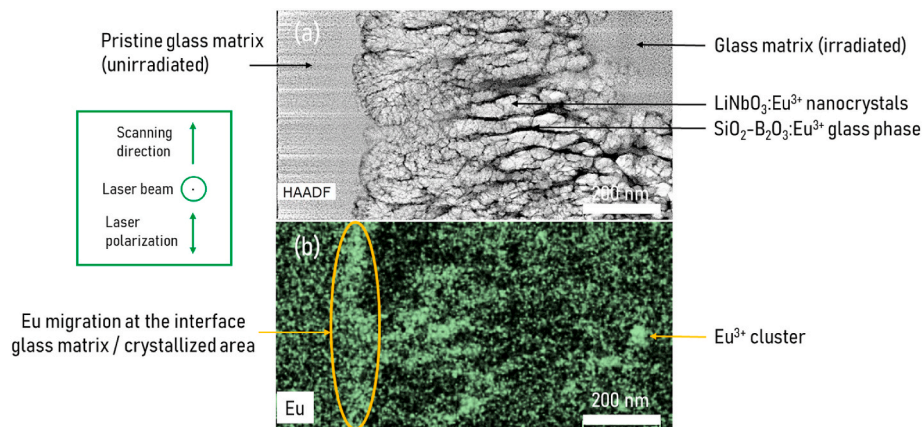


Fig. 3. (a) STEM high angle annular dark field (HAADF) image of LNSB1Eu irradiated area made at 1 μJ in the laser propagation direction. (b) STEM/EDS mapping of Eu^{3+} in (a) region. Fixed laser parameters: 1030 nm, 800 fs, NA 0.6, 200 kHz, 0° polarization, 10 $\mu\text{m/s}$ and 300 μm inscription depth.

Table 1

Absorption cross section σ_{abs} of Eu^{3+} ions, measured fluorescence lifetime τ_{rad} and emission cross section σ_{em} at 615 and 542 nm for the LNSB:Eu³⁺ doped glasses and irradiated areas at 1 μJ . Fixed laser parameters: 1030 nm, 800 fs, NA = 0.6, 200 kHz, 0° polarization, 10 $\mu\text{m/s}$ and 300 μm inscription depth.

Probed area and glass composition		σ_{abs}^a (10^{-20} cm ²) at 394/400/465 nm	τ_{rad} at 615 nm (μs) ± 0.1	σ_{em} at 615 nm (10^{-21} cm ²)	τ_{rad} at 542 nm (μs) ± 0.1	σ_{em} at 542 nm (10^{-20} cm ²)
Glass matrix	LNSB0.5Eu	1.20/0.20/0.53	769.4	3.9	10.5	17.2
	LNSB1Eu	1.33/0.21/0.58	768.1	3.8	11.7	15.0
	LNSB2Eu	1.56/0.26/0.66	742.7	3.9	10.5	11.4
Irradiated area	LNSB0.5Eu	–	690.7	4.2	9.8	19.2
	LNSB1Eu	–	623.4	4.6	11.2	15.7
	LNSB2Eu	–	583.9	4.7	10.2	13.0

^a σ_{abs} is calculated using the relations: $\sigma_{\text{abs}}(\lambda) = \frac{\alpha(\lambda)}{N}$, $\alpha(\lambda) = \frac{A(\lambda) \ln(10)}{e}$ and $N = \frac{c}{100} \frac{N_A d}{M}$, where N is the number of Eu^{3+} ions per cm³. A(λ) the absorbance, e the sample thickness, c the Eu^{3+} concentration, N_A the Avogadro constant, M the molar mass of Eu^{3+} and d the densities of the glasses, i.e. experimental values of 3.55, 3.57 and 3.61 \pm 0.01 for respectively LNSB0.5Eu, LNSB1Eu and LNSB2Eu.

local environment of Eu^{3+} ions. The relatively small differences in lifetime values are attributed to variation of the doping concentration, as we assume the phonon energies of the three doped LNSB:Eu³⁺ glasses to be similar. The decrease of lifetimes when Eu^{3+} concentration increases confirms the significance of the doping rate. The increasing of Eu^{3+} concentration also increases the non-radiative transition probabilities thus quenching the emissions (especially at 542 nm) and decreases their respective lifetimes.

The increase of luminescence intensity at 591 nm (⁵D₀ → ⁷F₁ magnetic dipole transition) for lower Eu^{3+} concentrations shows that the ions are in a more isotropic local environment for the 0.5 mol.% Eu^{3+} doping rate. Oppositely, the increase of Eu^{3+} in LNSB:Eu³⁺ glasses breaks the symmetry surrounding the ions, thus leading to fluorescence quenching at 591 nm from 0.5 to 2 mol.%.

4. Conclusion

Fabrication of femtosecond laser-induced nanocrystals in LNSB:Eu³⁺ glasses has been achieved. The nanostructures characterized by a lamellar crystalline phase made of LiNbO₃ (partially Eu^{3+} -doped) alternated with a SiO₂-B₂O₃ (partially Eu^{3+} -doped) glass phase can be oriented depending on the fs laser polarization during irradiation. Visible emission properties and elemental migration of Eu^{3+} ions have been determined into these oriented nanostructures induced by fs laser irradiation, while the ability to write luminescent nanostructures has been demonstrated. The irradiated area at 1 μJ is yielding to an enhancement of the luminescence intensity at 542 nm compared to the pristine glass, and the related lifetimes moderately decrease compared to their respective glass matrices.

Funding and acknowledgements

This work is supported by the French National Research Agency under the program CHARMMAT ANR-11-LABX-0039-grant. The authors would like to thank Maxime Vallet for his contribution on electronic microscopy imaging and analysis.

CRediT authorship contribution statement

Julien Ari: Investigation, Methodology, Formal analysis, Validation, Visualization, Data curation, Writing – original draft. **Maxime Vallet:** Writing – original draft, Writing – review & editing. **Maxime Cavillon:** Supervision, Project administration, Funding acquisition, Conceptualization, Writing – review & editing. **Olivier Plantevin:** Resources, Validation, Writing – review & editing. **Matthieu Lancry:** Resources, Project administration, Validation, Writing – review & editing. **Bertrand Pommellec:** Resources, Funding acquisition, Validation, Writing – review & editing.

Declaration of competing interest

The authors declare that they have no known competing financial interests or personal relationships that could have appeared to influence the work reported in this paper.

References

- [1] A.S. Lipat'ev, G.Y. Shakhgil'dyan, M.P. Vetchinnikov, S.V. Lotarev, T.O. Lipat'ieva, V.N. Sigaev, *Glass and Ceramics*, 2021.
- [2] L. Li, W. Wang, J. Tang, Y. Wang, J. Liu, L. Huang, Y. Wang, F. Guo, J. Wang, W. Shen, L.A. Belfiore, *Nanoscale Res. Lett.* 14 (2019) 190.
- [3] M. Zacharias, J. Heitmann, R. Scholz, U. Kahler, M. Schmidt, J. Bläsing, *Appl. Phys. Lett.* 80 (2002) 661–663.
- [4] I.M. Pinatti, A.F. Gouveia, C. Doñate-Buendía, G. Mínguez-Vega, J. Andrés, E. Longo, *Sci. Rep.* 10 (2020) 4613.
- [5] K. Sun, D. Tan, X. Fang, X. Xia, D. Lin, J. Song, Y. Lin, Z. Liu, M. Gu, Y. Yue, J. Qiu, *Science* 375 (2022) 307–310.
- [6] L. Yu, M. Nogami, *J. Alloys Compd.* 462 (2008) 187–191.
- [7] B. Zhu, Y. Dai, H. Ma, S. Zhang, G. Lin, J. Qiu, *Opt Express* 15 (2007) 6069–6074.
- [8] Y. Petit, G. Galleani, G. Raffy, J.-C. Desmoulin, V. Jubéra, A. Del Guerzo, A.S.S. de Camargo, L. Canioni, T. Cardinal, *Crystals* 11 (2021) 148.
- [9] S. Lee, M. Lee, K. Lim, *J. Lumin.* 122–123 (2007) 990–992.
- [10] C. Fan, B. Pommellec, R. Desmarchelier, H. Zeng, B. Bourguignon, G. Chen, M. Lancry, *Appl. Phys. B* 117 (2014) 737–747.
- [11] Y. Shimotsuma, P.G. Kazansky, J.R. Qiu, K. Hirao, *Phys. Rev. Lett.* 91 (2003), 247405.
- [12] E. Muzi, M. Cavillon, M. Lancry, F. Brisset, R. Que, D. Pugliese, D. Janner, B. Pommellec, *Crystals* 11 (2021).
- [13] E. Muzi, M. Cavillon, M. Lancry, F. Brisset, B. Sapaly, D. Janner, B. Pommellec, *Opt. Mater. Express* 11 (2021) 1313–1320.
- [14] J. Cao, M. Lancry, F. Brisset, L. Mazerolles, R. Saint-Martin, B. Pommellec, *Cryst. Growth Des.* 19 (2019) 2189–2205.
- [15] J. Cao, B. Pommellec, F. Brisset, A.-L. Helbert, M. Lancry, *J. Opt. Soc. Am. B* 33 (2016) 741–747.
- [16] J. Kaewkhao, K. Boonin, P. Yasaka, H.J. Kim, *Mater. Res. Bull.* 71 (2015) 37–41.
- [17] P. Aryal, C.R. Kesavulu, H.J. Kim, S.W. Lee, S.J. Kang, J. Kaewkhao, N. Chanthima, B. Damdee, *J. Rare Earths* 36 (2018) 482–491.
- [18] H. Song, S. Lu, S. E. R. Gao, J. Zhang, B. Chen, H. Xia, J. Zhang, Q. Ni, *J. Appl. Phys.* 91 (2002) 2959–2964.
- [19] K. Binnemans, *Coord. Chem. Rev.* 295 (2015) 1–45.
- [20] J. Qiu, K. Kojima, K. Miura, T. Mitsuyu, K. Hirao, *Opt Lett.* 24 (1999) 786–788.
- [21] K.S. Lim, S. Lee, M.T. Trinh, S.H. Kim, M. Lee, D.S. Hamilton, G.N. Gibson, *J. Lumin.* 122 (2007) 14–16.
- [22] W. Krupke, *IEEE J. Quant. Electron.* 10 (1974) 450–457.
- [23] T. Aitasalo, J. Hölsä, H. Jungner, M. Lastusaari, J. Niittykoski, *J. Phys. Chem. B* 110 (2006) 4589–4598.
- [24] K. Van den Eeckhout, P.F. Smet, D. Poelman, *Materials* 3 (2010) 2536–2566.
- [25] S. Liu, G. Zhao, W. Ruan, Z. Yao, T. Xie, J. Jin, H. Ying, J. Wang, G. Han, *J. Am. Ceram. Soc.* 91 (2008) 2740–2742.
- [26] H. Liang, Q. Zeng, Y. Tao, S. Wang, Q. Su, *Mater. Sci. Eng., B* 98 (2003) 213–219.
- [27] B.K. Grandhe, V.R. Bandi, K. Jang, S.-S. Kim, D.-S. Shin, Y.-I. Lee, J.-M. Lim, T. Song, *J. Alloys Compd.* 509 (2011) 7937–7942.
- [28] T.T. Fernandez, M. Sakakura, S.M. Eaton, B. Sotillo, J. Siegel, J. Solis, Y. Shimotsuma, K. Miura, *Prog. Mater. Sci.* 94 (2018) 68–113.
- [29] J. Cao, B. Pommellec, F. Brisset, M. Lancry, *Opt Express* 26 (2018) 7460–7474.
- [30] A. Herrmann, S. Fibikar, D. Ehrhart, *J. Non-Cryst. Solids* 355 (2009) 2093–2101.
- [31] A. Sreenivasulu, S. Buddhudu, *Trans. Indian Ceram. Soc.* 67 (2008) 129–138.